


Targeting glucose-6-phosphate dehydrogenase by 6-AN induces ROS-mediated autophagic cell death in breast cancer

Yin Li¹, Fangxu Zheng¹, Yupeng Zhang¹, Zhoujun Lin¹, Juan Yang¹, Xiao Han¹, Ya Feng¹, Xiaolin Pei¹, Fei Li¹, Qiao Liu¹, Lizhong Yan¹, Tianjiao Li¹, Yifan Zhang¹, Ding Li², Zhenkun Fu^{1,3}, Changjun Wang⁴, Qiang Sun⁴ and Chenggang Li¹ 

1 State Key Laboratory of Medicinal Chemical Biology and College of Pharmacy, Nankai University, Tianjin, China

2 Department of Clinical Laboratory, Tianjin Medical University Cancer Institute and Hospital, China

3 Department of Immunology & Wu Lien-Teh Institute & Heilongjiang Provincial Key Laboratory for Infection and Immunity, Harbin Medical University & Heilongjiang Academy of Medical Science, China

4 Department of Breast Surgery, Peking Union Medical College Hospital, Beijing, China

Keywords

6-AN; autophagy; breast cancer; G6PD; PPP

Correspondence

C. Li, State Key Laboratory of Medicinal Chemical Biology and College of Pharmacy, Nankai University, No.38 Tongyan Road, Jinnan District, Tianjin 300350, China
Tel: 17720137434

E-mail: lichenggang@nankai.edu.cn

C. Wang and Q. Sun, Department of Breast Surgery, Peking Union Medical College Hospital, No.1 Shuaifuyuan, Dongcheng District, Beijing 100730, China
Tel: +8610-69152706 (CW); 13261258293 (QS)

E-mail: wangchangjun@pumch.cn (CW); sunqiang@pumch.cn (QS)

(Received 15 March 2022, revised 28 June 2022, accepted 31 August 2022)

doi:10.1111/febs.16614

Dysregulation of G6PD involved in the pentose phosphate pathway (PPP) is known to promote tumorigenesis. The PPP plays a pivotal role in meeting the anabolic demands of cancer cells. However, the detailed underlying molecular mechanisms of targeting the G6PD-regulated PPP in breast cancer remain unclear. In this study, we aimed to elucidate the molecular pathways mediating the effects of G6PD on cancer progression. Clinical sample analysis found that the expression of G6PD in breast cancer patients was higher than that in normal controls, and patients with higher G6PD expression had poor survival. Gene knockdown or inhibition of G6PD by 6-AN in MCF-7 and MDA-MB-231 cells significantly decreased cell viability, migration, and colony formation ability. G6PD enzyme activity was inhibited by 6-AN treatment, which caused a transient upregulation of ROS. The elevated ROS was independent of cell apoptosis and thus associated with abnormal activated autophagy. Accumulated ROS levels induced autophagic cell death in breast cancer. Inhibition of G6PD suppresses tumour growth in preclinical models of breast cancer. Our results indicate that targeting the G6PD-regulated PPP could restrain tumours *in vitro* and *in vivo*, inhibiting G6PD caused cell death by over-activating autophagy, therefore leading to inhibited proliferation and tumour formation.

Introduction

Breast cancer has the highest incidence among all female malignancies and remains one of the leading causes of cancer-related death [1]. Certain factors

increase the risk of breast cancer, including oestrogen exposure, alcohol consumption, and metabolic syndrome. Metabolic syndrome, which includes

Abbreviations

6-AN, 6-aminonicotinamide; DAPI, 4',6-diamidino-2-phenylindole; DMSO, dimethyl sulphoxide; ER α , oestrogen receptor α ; FBS, fetal bovine serum; G6PD, glucose-6-phosphate dehydrogenase; GFP, green fluorescent protein; GSH, glutathione; H&E, haematoxylin and eosin; HMOX1, heme oxygenase 1; MCF-7, ER+ human breast cancer cell line; MDA-MB-231, triple negative human breast cancer cell line; MTT, thiazolyl blue; NADPH, reduced nicotinamide adenine dinucleotide phosphate; NFE2L2, nuclear factor erythroid-2 related factor; PBS, phosphate-buffered saline; PPP, pentose phosphate pathway; PR, progesterone receptor; q-PCR, quantitative polymerase chain reaction; ROS, reactive oxygen species.

dyslipidemia, hypertension, and type 2 diabetes, was proven to have a strong correlation with increased breast cancer risk [2,3]. However, the underlying mechanisms remain elusive.

Cancer cells change their metabolic signatures to meet the demand for macromolecules, support high proliferation rates, and respond to oxidative stress. As an important branch of glucose metabolism, the pentose phosphate pathway (PPP) plays an important role in biosynthesis. The main significance of the PPP is (a) to provide ribose as a raw material of DNA synthesis and (b) to produce a large amount of NADPH as the hydrogen donor to satisfy the needs of anabolic tissues and maintain redox balance. Despite the vital biological function of the PPP, its regulatory mechanism in cancer development is not fully understood. Glucose-6-phosphate dehydrogenase (G6PD) is a preliminary rate-limiting enzyme in the PPP. It is upregulated in various tumours and is essential for tumour cell proliferation and metastasis. Studies have shown that high G6PD expression is a poor prognostic factor in bladder cancer, and the levels of G6PD expression increase with increasing tumour stage. Bladder cancer patients with high G6PD expression had worse survival rates than those with lower G6PD expression [4]. TAp73 increases PPP flux by activating the expression of G6PD and directs glucose to NADPH and ribose production for macromolecule synthesis and reactive oxygen species (ROS) removal [5]. YY1 stimulates the PPP by activating G6PD, promoting the production of nucleotides and DNA synthesis, reducing ROS levels, and providing increased reducing capacity in the form of NADPH to intensify antioxidant defence [6].

Hence, this implies that G6PD may play a crucial role in tumorigenesis. However, there are fewer studies on G6PD in breast cancer, especially triple-negative breast cancer. Here, we show that 6-aminonicotinamide (6-AN) inhibits G6PD to alter the autophagic flux of tumour cells and induce autophagy, thereby inhibiting the development of breast cancer. Therefore, G6PD may be a promising therapeutic target for breast cancer.

Results

Identification of abnormally activated G6PD in breast cancer

Published studies have shown that G6PD is highly expressed in a variety of tumours [7,8]. To investigate the expression of G6PD in breast cancer, we evaluated *G6PD* gene expression in cancerous and noncancerous mammary tissues on the StarBase website ([https://](https://starbase.sysu.edu.cn/)

starbase.sysu.edu.cn/). We detected overexpression of *G6PD* in breast cancers relative to normal breast tissues (Fig. 1A). Notably, we observed a marginally significantly poorer survival rate in breast cancer patients with G6PD overexpression (Fig. 1B). To further determine G6PD expression in breast cancer, q-PCR and immunoblot analysis of breast cancer cells were performed. The protein results showed that G6PD expression was elevated in MCF-7 cells compared with MCF-10A normal breast cells (Fig. 1C). The gene results showed that *G6PD* expression was elevated in MDA-MB-231 (MDA-231) and MCF-7 cells compared with MCF-10A normal breast cells (Fig. 1D). In addition, proteins and genes of G6PD were upregulated in breast cancer tissues compared to matched adjacent noncancerous tissues (Fig. 1E,F). Consistent with the results, IHC for breast cancer tissue samples revealed that G6PD protein levels were significantly increased in cancer tissue compared with matched adjacent normal tissue (Fig. 1G).

The abovementioned results suggest that G6PD expression was elevated in both breast cancer tissues and cells. G6PD is a crucial rate-limiting enzyme of the PPP [9]. However, it remains unclear how G6PD is involved in cell redox, particularly its impact on cancer cell growth and death. Our research strongly suggests that G6PD may be involved in breast cancer tumorigenesis, and we further investigated the underlying mechanism.

G6PD knockdown impaired tumorigenesis of breast cancer

To study the role of G6PD in the development and progression of breast cancer, we stably knocked down G6PD in MDA-231 and MCF-7 cells using lentiviral constructs to determine the G6PD knockdown efficiency (Fig. 2A). Silencing G6PD enhances the antitumor effects of oxaliplatin in colorectal cancer cells [10]. However, the experimental results showed that the change in apoptosis-related protein expression was not obvious in either cell line (Fig. 2B).

Metastasis is the main cause of breast cancer patient death and is highly related to cancer cell migration. A study by Hong-Sheng Zhang *et al.* [11] found that NFE2L2 promotes breast cancer cell proliferation and migration via upregulation of the G6PD/HIF-1 α /Notch1 signalling axis. Therefore, we sought to test whether G6PD knockdown affected the cell phenotype. We found that G6PD knockdown impacted cell viability, cell death, migratory behaviour, and colony formation ability compared with the control. The viability of G6PD knockdown cells was significantly

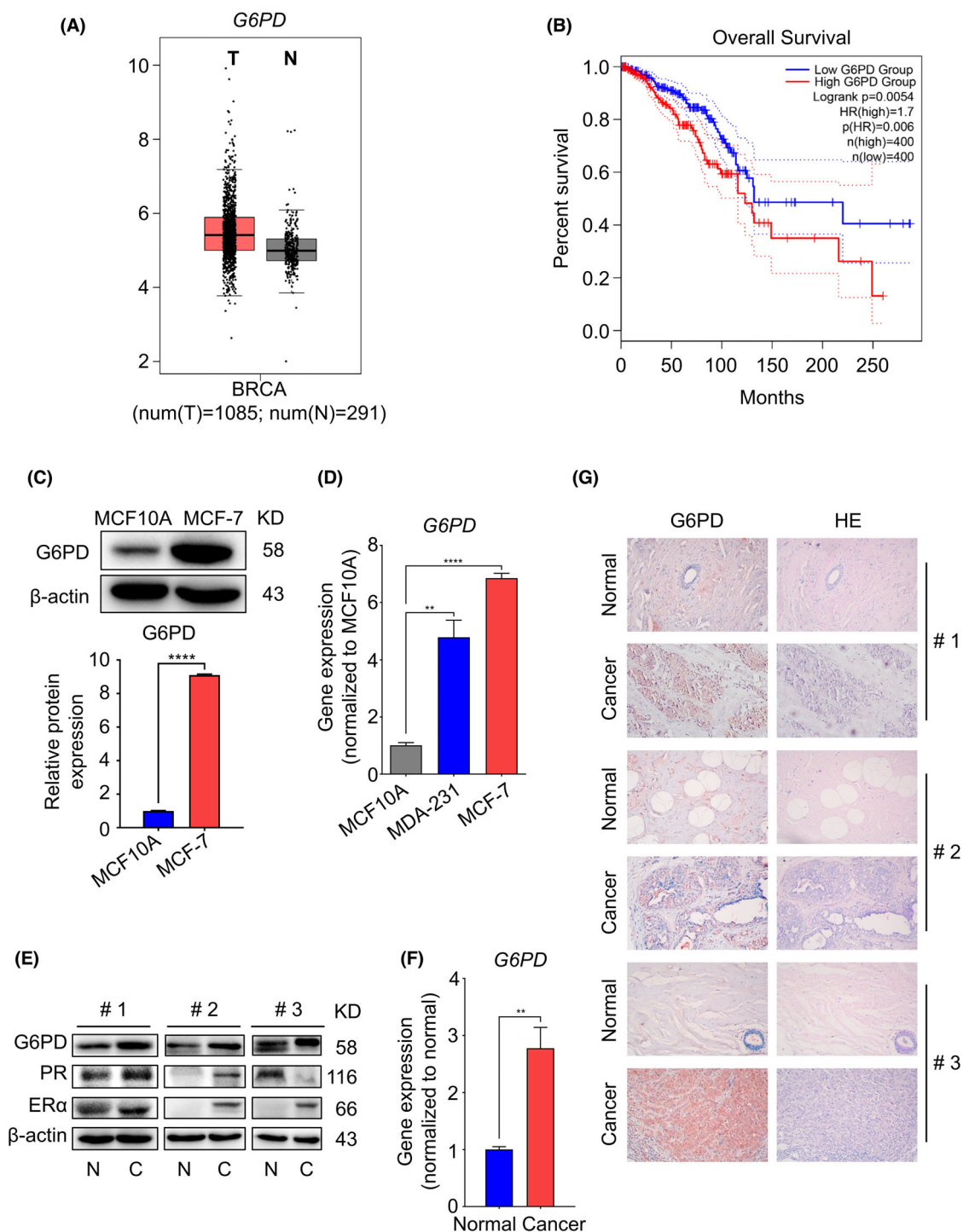


Fig. 1. Identification of abnormally activated G6PD in breast cancer. (A) Gene expression of *G6PD* in normal people ($n = 291$) and breast cancer patients ($n = 1085$) was analysed by the StarBase 3.0 website. (B) The relationship between G6PD expression and the survival rate in human samples [n (high) = 400, n (low) = 400] was analysed by the StarBase 3.0 website. (C) Immunoblot analyses of and G6PD in MCF-7 cells compared to MCF-10A cells. (D) q-PCR analysis of the transcription levels of *G6PD* in MDA-231 and MCF-7 cells compared to MCF-10A cells. (E) Immunoblot analyses of G6PD, PR, and ER α protein in breast cancer patients compared to normal people (N: Normal, C: Cancer). (F) Transcription levels of *G6PD* were measured using q-PCR on mRNA prepared from breast cancer patients and normal breast samples. (G) IHC staining detected G6PD in breast cancer tissue and paracarcinoma tissue in humans. 200 \times magnification. $**P < 0.01$, $****P < 0.001$.

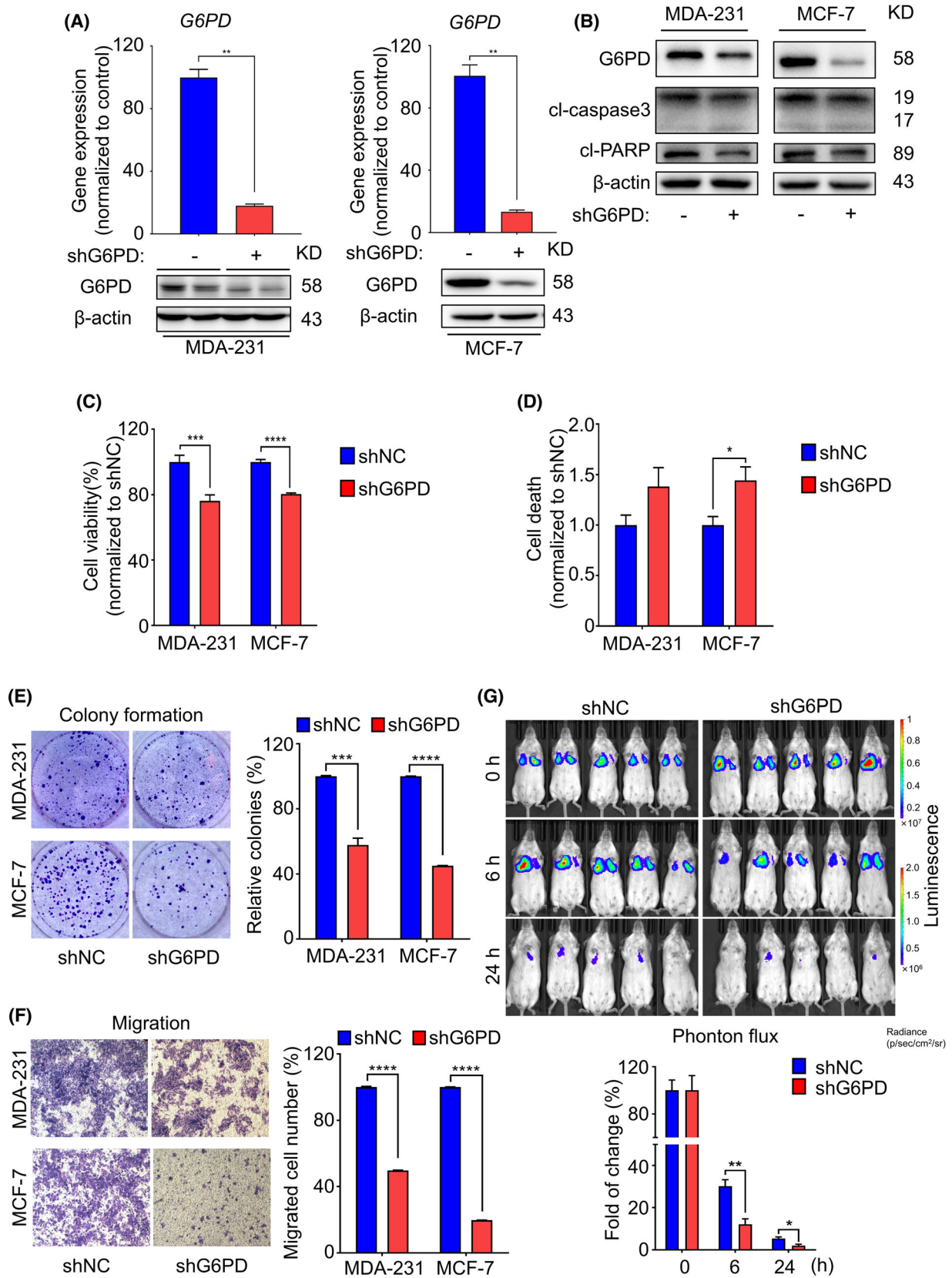


Fig. 2. G6PD knockdown impaired tumorigenesis of breast cancer. (A) G6PD knockdown efficiency was validated on G6PD gene and protein expression in MDA-231 and MCF-7 cells by q-PCR and Western blotting, respectively. (B) Immunoblot analysis of the changes in G6PD, cl-caspase3, and cl-PARP in MDA-231-shG6PD and MCF-7-shG6PD cells. (C) Viability of MDA-231-shG6PD and MCF-7-shG6PD cells was measured by MTT assay following 24 h. (D) Cell death of MDA-231-shG6PD and MCF-7-shG6PD cells was determined with the PI exclusion assay following 24 h. (E, F) The effect of G6PD knockdown in MDA-231 and MCF-7 cells was investigated by colony formation assay. Images were taken with 4× magnification (E) and Transwell assay for cell migration. Images were taken with 40× magnification (F). (G) Lung colonization was measured using bioluminescence at 0, 6, and 24 h after injection ($n = 5$). Luminescence colour scale: 0 h (min = 1×10^6 , max = 1×10^7) and 6 and 24 h (min = 2×10^5 , max = 2×10^6). * $P < 0.05$, ** $P < 0.01$, *** $P < 0.001$, and **** $P < 0.0001$.

lower than that of the vector control cells, and the death rate of G6PD knockdown cells was significantly higher than that of the control (Fig. 2C,D). We observed that knockdown of G6PD impeded the colony formation capacity and migratory capability (Fig. 2E,F).

To further investigate the role of G6PD *in vivo*, MDA-231-shNC-luciferase and MDA-231-shG6PD-luciferase cells were intravenously injected into BALB/c mice for lung colonization assay. At different time points post-cell inoculation, we observed that the decreasing rate of fluorescence intensity in the shG6PD group was faster than that in the control group (Fig. 2G). These data suggest that G6PD knockdown compromises the survival and progress of breast cancer cells *in vivo* and *in vitro*.

Pharmacological inhibition of G6PD by 6-AN blocked cell survival, migration, and colony formation

The abovementioned research focused on the regulation of G6PD by molecular biological means. Next, we sought to investigate the regulation of G6PD activity in the PPP via pharmacologic inhibition. Currently, 6-AN, polydatin, zoledronic acid, and steroids are the commonly used inhibitors of G6PD [12–15]. Given that zoledronic acid indirectly suppresses G6PD upstream, 6-AN could be a better agent due to its analogy to NADP and direct interaction with G6PD as an antagonist. 6-AN exhibits weaker inhibitory effects in G6PD knockdown cells than in the control group. In addition, 6-AN induced a concentration-dependent decrease in cell viability, and cells were insensitive to 6-AN due to G6PD knockdown and loss of its target (Fig. 3A). Similarly, to detect whether apoptosis was triggered by 6-AN, MDA-231 and MCF-7 cells were treated with different concentrations of 6-AN for 24 h. However, Western blotting analysis showed that 6-AN did not induced apoptosis protein accumulation (Fig. 3B). After 6-AN treatment for 24 h, 6-AN decreased breast cancer cell viability but had no effect on 293T cells, which was used as a control (Fig. 3C). The death rate of 6-AN treatment was

significantly higher than that of the control in MDA-231 and MCF-7 cells (Fig. 3D). Subsequently, we selected the optimal concentration of 6-AN to analyse G6PD expression level changes. Likewise, 6-AN did not significantly affect the G6PD gene (Fig. 3E) and protein (Fig. 3B) expression in both MDA-231 and MCF-7 cells. Our results indicate that 6-AN treatment results in a decrease in PPP flux and that 6-AN observably affects the viability of breast cancer cells but does not induce apoptosis in MDA-231 and MCF-7 cells.

Although 6-AN is a specific inhibitor of G6PD, it does not affect the protein and gene expression of G6PD in MDA-231 and MCF-7 cells. Therefore, breast cancer cells were assayed for G6PD enzyme activity after 6-AN treatment. The results showed low G6PD enzymatic activity after 6-AN treatment for 24 h (Fig. 3F). Inhibition of either G6PD enzymatic activity or protein expression could obstruct the PPP [16,17]. We further investigated whether the specific inhibition of G6PD in breast cancer cells restrains their migration and colony formation (Fig. 3G,H). The results indicate that 6-AN does not affect the transcriptional and translational levels of G6PD but influences its enzymatic activity, therefore facilitating cell death and inhibiting the migration and colony formation ability of breast cancer cells.

6-AN treatment induces autophagic cell death by accumulating ROS in G6PD-overactivated breast cancer

Impaired G6PD activity by high glucose concentrations induced apoptosis in MIN6 β cells [18]. To elucidate the mechanism underlying the impairment of G6PD on cell viability, we assessed the G6PD inhibition on the apoptosis of breast cancer cells. Flow cytometry analysis revealed that after 24 h of treatment, 6-AN did not significantly change the cell apoptosis rate, while H_2O_2 successfully induced apoptosis as a positive control (Fig. 4A). Cell death occurs in three ways: necrosis, apoptosis, and autophagy. Evidence is emerging that G6PD blockade enhances the inhibitory effect of tyrosine kinase in MCF-7 cells

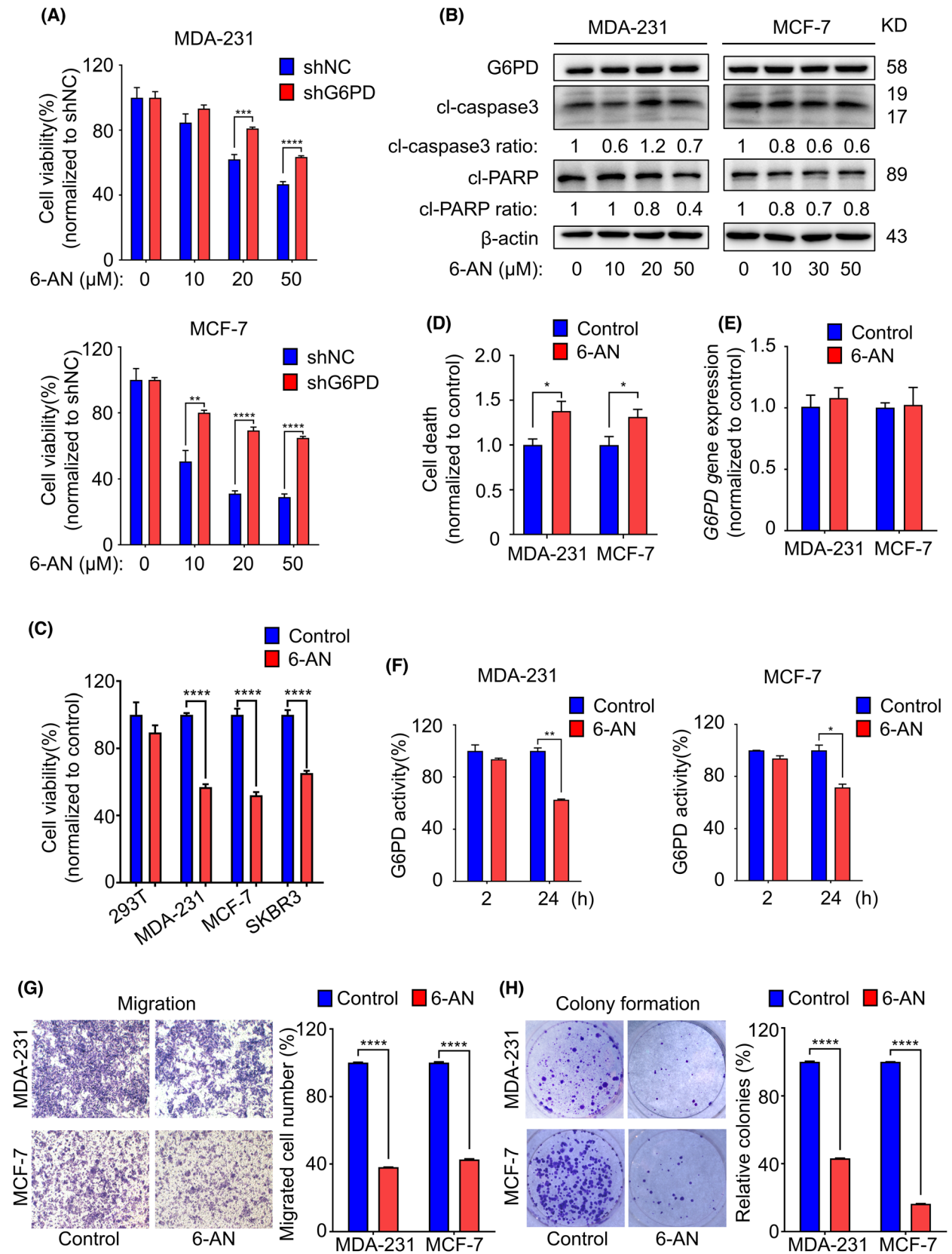


Fig. 3. Pharmacological inhibition of G6PD by 6-AN blocked cell survival, migration and colony formation. (A) MDA-231 and MCF-7 cells were treated with different concentrations of 6-AN for 24 h. cell viability was measured using MTT. (B) MDA-231 and MCF-7 cells were treated with different concentrations of 6-AN for 24 h. Immunoblot analysis of the protein changes in G6PD, cl-caspase 3, and cl-PARP. (C) MDA-231, MCF-7, SKBR3, and 293T cells were treated with 6-AN (10 μM) for 24 h, and cell viability was measured with MTT. (D) Cells were treated with 6-AN for 48 h. Cell death was determined with the PI assay. (E) Cells were treated with 6-AN for 24 h. Gene expression of *G6PD* was measured using q-PCR. (F) Cells were treated with 6-AN for 2 or 24 h. G6PD was detected by the enzyme activity kit. (G, H) The effect of 6-AN on the migration and colony formation was investigated by Transwell assay. Images were taken with 40 \times magnification (G) and colony formation assay. Images were taken with 4 \times magnification (H). (D–H) 6-AN was used 20 μM for MDA-231 and 30 μM for MCF-7. * $P < 0.05$, ** $P < 0.01$, *** $P < 0.001$, and **** $P < 0.0001$.

through autophagy interference [19]. Therefore, we intended to determine whether 6-AN mediates G6PD-induced autophagy. The autophagic signal intensity was positively correlated with the LC3-II/LC3-I ratio. Immunoblot analysis showed that autophagy was activated by incubation with 6-AN for 24 h in MDA-231 and MCF-7 cells irrespective of 6-AN concentration, and phospho-S6 and phospho-4EBP1 protein levels were reduced, indicating decreased proliferation and retarded growth after 6-AN treatment. Different cell lines drew a similar conclusion (Fig. 4B). In addition to the autophagy level quantitatively measured by immunoblotting, we further examined autophagic flux by confocal microscopy in MDA-231 cells transiently transfected with the GFP-RFP-LC3 fusion plasmid. Under a low pH environment, GFP-labelled autophagosomes lost their fluorescence, while acid-insensitive RFP remained positive. The GFP/RFP ratio was used here to determine the state of autophagy flow. Rapamycin (Rapa), an autophagy agonist, could activate autophagy by inhibiting the mammalian target of mTORC1. The fluorescence intensity of GFP/RFP decreased in cells treated with 6-AN or rapamycin for 24 h. The results indicated that 6-AN treatment improved autophagic flux, inducing autophagic death in MDA-231 cells (Fig. 4C,D). Chloroquine (CQ), an autophagy inhibitor, inhibits the fusion of autophagosomes and lysosomes by increasing lysosomal pH, led to the accumulation of autophagosomes and the upregulation of LC3-II and phospho-62. To determine whether 6-AN triggers cell death by regulating autophagy, we compared the autophagy levels with rapamycin and CQ treatments. MDA-231 and MCF-7 cells were pretreated with CQ or rapamycin for 1 h to inhibit or activate autophagy, and then 6-AN was added for 6 h. The results showed that the level of phospho-62 was increased in the 6-AN with the CQ group and was decreased in the 6-AN plus rapamycin group compared with the 6-AN group, indicating successful abrogation or activation of autophagy, further suggesting that 6-AN could indeed regulate autophagy, inhibit cell growth and proliferation, and cause autophagic cell death (Fig. 4E). After pre-treatment with

CQ, treatment with CQ rescued cell viability in MDA-231 and MCF-7 compared to 6-AN alone (Fig. 4F). And, the combinational treatment rescued cell death in MDA-231 and MCF-7 compared to 6-AN alone (Fig. 4G). These results suggest that autophagy inhibition by CQ can attenuate 6-AN induced cell viability and death, thereby indicating that 6-AN-induced autophagy contributed to breast cancer cell death. Consistent with *in vitro* findings above, expressions of *MAP1LC3A* and *MAP1LC3B* were decreased in breast cancer compared with those of normal breast tissue. Appropriately, *SQSTM1/P62* expression was increased, suggesting impaired autophagy level in breast cancer (Fig. 4H). In addition, we observed significant accumulation of phospho-62 protein in breast cancer sections compared with adjacent non-tumour tissues, indicating that autophagy inhibited in breast cancer tissues (Fig. 4I). Thereafter, stimulation of autophagy in breast cancer may induce cell death. These findings demonstrated that 6-AN exerted its antiproliferative and antimigratory effects through the activation of autophagic cell death.

Theoretically, inhibition of G6PD activity might limit the conversion of NADP^+ into NADPH. One major function of NADPH is to scavenge ROS to maintain cellular redox balance and protect against oxidative stress. A publication reported that G6PD deficiency promotes ROS accumulation and decreases NO bioavailability in endothelial cells [20]. To investigate the level of ROS in breast cancer, we evaluated *HMOX1* and *NFE2L2* gene expression in cancerous and noncancerous mammary tissues. We found that *HMOX1* expression was higher in breast cancer tissue than in normal breast tissue, but the expression of *NFE2L2* was decreased. *HMOX1* and *NFE2L2* work together to maintain the normal physiological level of ROS (Fig. 5A). Next, we investigated the ROS and autophagy alterations caused by G6PD knockdown. G6PD knockdown leads to ROS accumulation, and G6PD over-expression rescued the ROS level in MDA-231 and MCF-7 G6PD knockdown cells (Fig. 5B). N-acetyl-l-cysteine (NAC) is a potent ROS scavenger that inhibits autophagic flux induced by

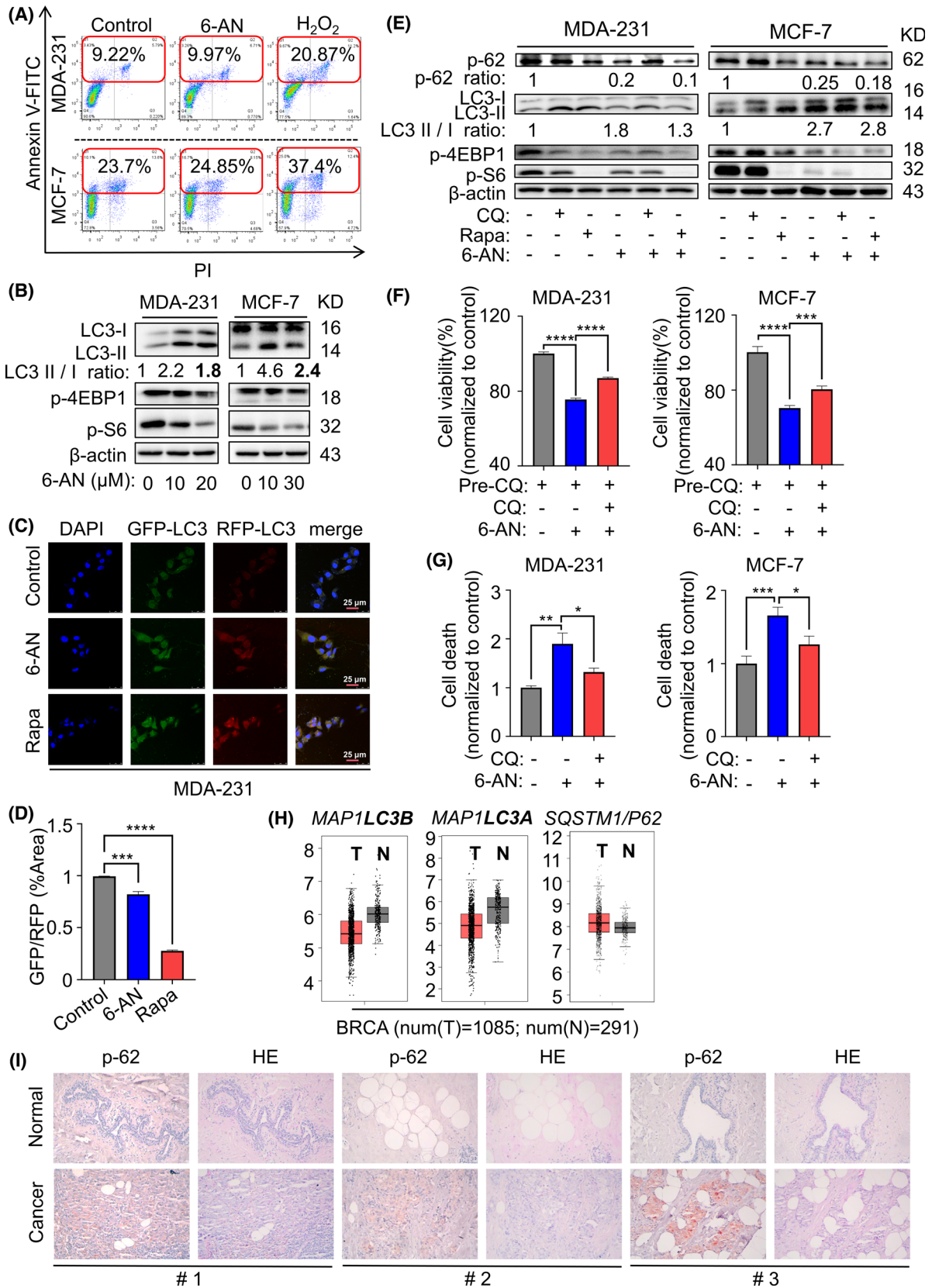


Fig. 4. 6-AN treatment induces autophagic cell death in G6PD-overactivated breast cancer. (A) Cell apoptosis was tested by flow cytometry assay of 6-AN (20 μM for MDA-231 and 30 μM for MCF-7) and H_2O_2 (30 μM for MCF-7 or 800 μM for MDA-231) treatment used as positive control. (B) Levels of LC3B, phospho-S6, and phospho-4EBP1 were assessed by immunoblotting. (C, D) Autophagy flux in GFP-RFP-LC3-labelled MDA-231 cells was detected by confocal microscopy after treatment with 6-AN (20 μM) and rapamycin (Rapa) (20 nM). (E) Levels of LC3B, phospho-62, phospho-S6, and phospho-4EBP1 were assessed by immunoblotting. (F) First, pre-treatment with CQ for 6 h and then MDA-231 and MCF-7 cells were treated with 6-AN or 6-AN plus CQ for 24 h. cell viability was measured with MTT. (G) MDA-231 and MCF-7 cells were treated with 6-AN or 6-AN plus CQ for 24 h. cell death was determined with the PI assay. (E–G) 6-AN was used with 20 μM for MDA-231 and 30 μM for MCF-7. CQ and Rapa added with 10 μM and 20 nM, respectively. (H) The gene expression of *MAP1LC3A*, *MAP1LC3B*, and *SQSTM1/P62* in normal people ($n = 291$) and breast cancer patients ($n = 1085$) was analysed by the StarBase 3.0 website. (I) IHC staining analyses of phospho-62 in breast cancer tissue and paracarcinoma tissue in humans. 200 \times magnification. * $P < 0.05$, ** $P < 0.01$, *** $P < 0.001$, **** $P < 0.0001$.

H_2O_2 [21]. G6PD-knockdown MDA-231 and MCF-7 cells were pretreated with H_2O_2 for 30 min to induce ROS first, and then the ROS scavenger NAC was added for 2 h. We found that treatment with NAC markedly attenuated the induction of autophagy by G6PD knockdown, indicating that ROS could promote autophagy (Fig. 5C,D). Following a few preliminary experiments, intracellular ROS production was measured by flow cytometry. ROS levels returned to base levels at 24 h after a transient increase at 2 h with treatment of 6-AN in MDA-231 and MCF-7 cells (Fig. 5E). G6PD-overexpressing INS-1 insulinoma cells increase ROS accumulation and promote the expression of several peroxidase genes, such as iNOS and NADPH oxidase [22]. Another study suggested that G6PD inhibition by 6-AN leads to alleviation of acute lung injury induced by LPS due to reduction in NOX2-derived ROS [23]. G6PD-deficient endothelial cells exhibit decreased eNOS, NO, and GSH levels [24]. Then, we tested the GSH changes in MDA-231 and MCF-7 cells after 6-AN treatment for 2 and 24 h. The data showed that the total GSH did not significantly change at 2 h but decreased by approximately half at 24 h (Fig. 5F). Upregulation of antioxidant genes was observed in G6PD-deficient mice [25]. In our study, there was no significant change in the *NFE2L2* and *HMOX1* gene expression levels after 2 h of 6-AN incubation, while there was a significant increase at 24 h (Fig. 5G). Collectively, these results suggest that the slight increase in ROS at 2 h after 6-AN was probably attributed to the delayed cell response by using GSH or highly expressing *NFE2L2* and *HMOX1* to combat oxidative insults. This hypothesis was proven by the fact that GSH, *NFE2L2*, and *HMOX1* transcription levels did not change significantly at 2 h, and *NFE2L2* and *HMOX1* transcription levels increased as ROS decreased at 24 h due to the activation of cell antioxidation reactions.

A link between autophagy and ROS production has been observed. ROS-induced autophagy regulates the apoptosis and proliferation of porcine trophoblast cells

[21]. Therefore, we first determined whether autophagy is associated with upregulated ROS levels. MDA-231 and MCF-7 cells were treated with Rosup (the ROS-activated agent from the kit) for 2 h or H_2O_2 for 24 h and analysed for the expression of genes involved in autophagy (Fig. 5H). Our results demonstrated that autophagy was activated after treatment with 6-AN or the positive control, and autophagy may be induced by enhanced ROS levels. Furthermore, NAC was used in combination with 6-AN to determine whether 6-AN mediates ROS-induced autophagic flux. After 30 min of pretreatment with NAC, we treated MDA-231 and MCF-7 cells with 6-AN or 6-AN plus NAC for 2 h. We found that NAC rescued 6AN-induced autophagy (Fig. 5I). In addition, to prove the hypothesis that G6PD helps eliminate ROS, we overexpressed G6PD in MCF-10A cells, and *G6PD* expression was increased by approximately 0.12 million-fold (Fig. 5J), accompanied by significantly increased G6PD activity (Fig. 5K). NADPH is a key connector between G6PD and the ROS scavenging system. MCF-10A cells were stimulated with H_2O_2 for 30 min after G6PD overexpression, and G6PD-overexpressing cells had an enhanced ROS scavenging capacity compared with the control at 24 h (Fig. 5L). Next, we investigated the ROS and autophagy changes induced by G6PD overexpression. The antioxidant gene *NFE2L2* was significantly reduced in G6PD-overexpressing MCF-10A cells, and G6PD overexpression also led to low expression of autophagy-associated genes (Fig. 5M). And, autophagy and ROS were inhibited in G6PD-overexpressing MCF-10A cells (Fig. 5N). Above-mentioned data illustrated that targeting G6PD by 6-AN provokes oxidative stress due to clearance dysfunction and elicits autophagic cell death.

Inhibition of G6PD suppresses tumour growth in preclinical models of breast cancer

The preceding experiments demonstrated that targeting the G6PD-regulated PPP *in vitro* can inhibit cell

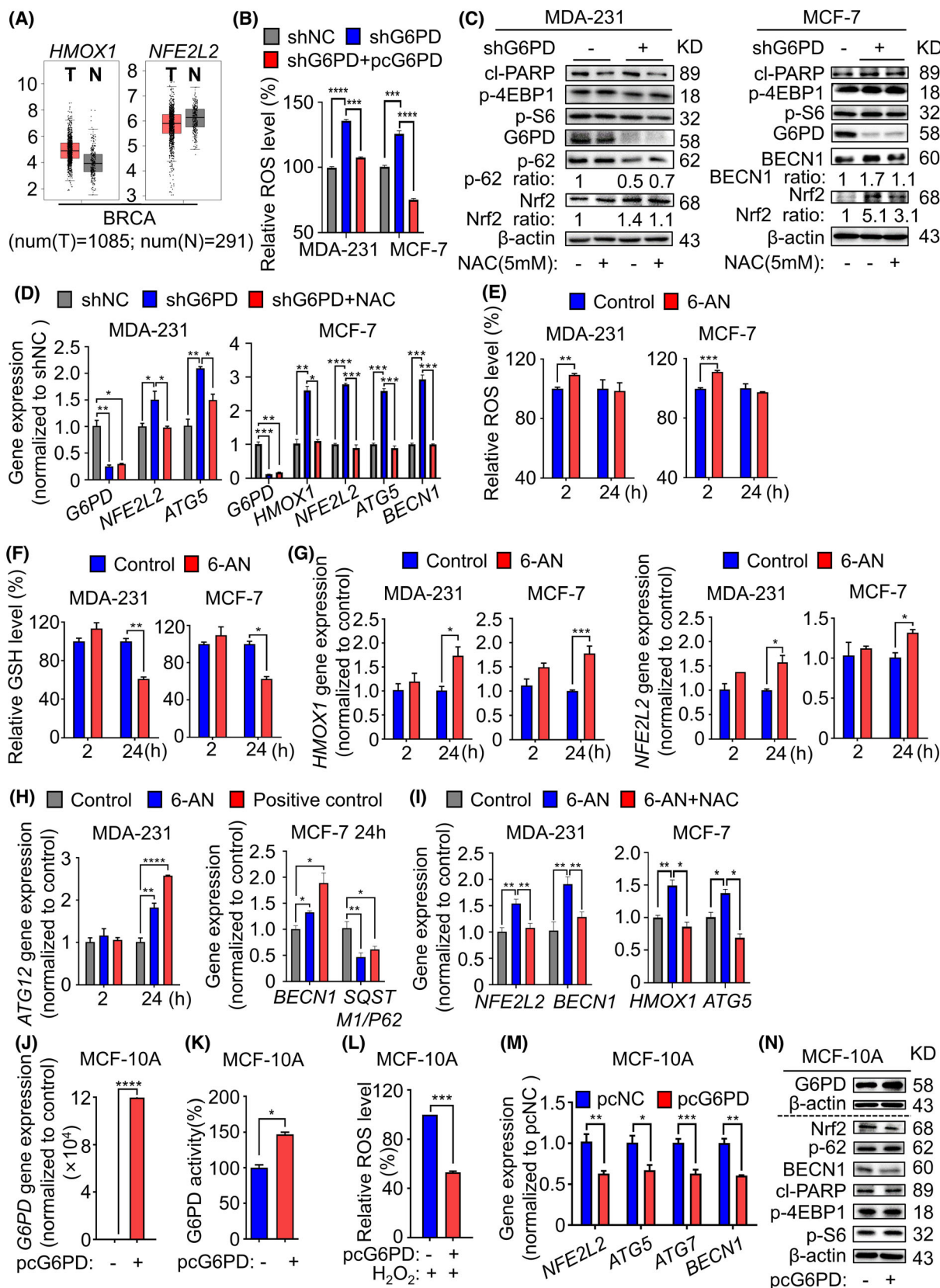


Fig. 5. Accumulated ROS levels induced autophagy in G6PD-inhibited breast cancer. (A) Gene expression of *HMOX1* and *NFE2L2* in normal people ($n = 291$) and breast cancer patients ($n = 1085$) was analysed by the StarBase 3.0 website. (B) Cellular ROS levels were measured by flow cytometry assay using DCFH-DA. (C, D) MDA-231 and MCF-7 cells were pretreated with H_2O_2 for 30 min and then treated with NAC (5 mM) for 2 h. Immunoblot analysis of G6PD, cl-PARP, phospho-S6, phospho-4EBP1, phospho-62, BECN1, and Nrf2 (C). Gene expression of *G6PD*, *NFE2L2*, *HMOX1*, *BECN1*, and *ATG5* were measured using q-PCR (D). (E–G) MDA-231 and MCF-7 cells were treated with 6-AN. Cellular ROS levels were measured by flow cytometry assay using DCFH-DA (E). Cellular GSH levels were measured by kit (F). *HMOX1* and *NFE2L2* were measured using q-PCR (G). (H) MDA-231 and MCF-7 cells were treated with 6-AN or positive control. Expression of autophagy-related genes were measured using q-PCR. (I) MDA-231 and MCF-7 cells were treated with 6-AN or 6-AN plus NAC (5 mM) for 2 h. *NFE2L2*, *HMOX1*, *BECN1*, and *ATG5* were measured using q-PCR. (E–I) 6-AN was used with 20 μ M for MDA-231 and 30 μ M for MCF-7. (J–N) MCF-10A cells were harvested after transfection of G6PD-overexpressing (pcG6PD) cells for 24 h. Gene expression of *G6PD* was measured using q-PCR (J). G6PD enzyme activity was studied using a G6PD enzyme activity detection kit (K). Cellular ROS levels measured by flow cytometry assay using DCFH-DA, which were treated with H_2O_2 (100 μ M) for 30 min (L). Gene expression of *NFE2L2*, *ATG5*, *ATG7* and *BECN1* was measured using q-PCR (M). G6PD, cl-PARP, phospho-S6, phospho-4EBP1, phospho-62, BECN1 and Nrf2 were detected by Western blotting (N). * $P < 0.05$, ** $P < 0.01$, *** $P < 0.001$, **** $P < 0.0001$.

viability, increase cell death, and decrease the migration and colony forming abilities of cells.

To further investigate whether G6PD knockdown affects breast cancer cell survival *in vivo*, equal amounts of MDA-231-shNC or MDA-231-shG6PD cells were injected into CD1 nude mouse flanks subcutaneously. Fourteen days later, tumours could be measured with a Vernier calliper every week. The G6PD-knockdown group exhibited a large reduction in tumour size and tumour growth (Fig. 6A). For immunohistochemical staining, tumour tissue was collected from three random mice per group, and G6PD, phospho-62, and Ki67 protein expression of the shG6PD group was reduced (Fig. 6B). As mentioned before, cellular ROS reduction is accompanied by a decrease in GSH. A significant positive correlation was observed between the ROS level and GSH content in breast cancer cells. *In vivo*, shG6PD tumour tissues showed an increased GSH level compared to that in control tissues (Fig. 6C). In other words, ROS aberrantly accumulated in the shG6PD group. In addition, we found that the gene expression of *G6PD* was decreased in the G6PD knockdown group, and autophagy-related gene 7 (*ATG7*) was increased (Fig. 6D). G6PD knockdown caused an increase in the autophagy-related protein BECN1 (Fig. 6E). The results suggest that G6PD knockdown attenuates cell viability *in vivo* by inducing autophagic death. The average tumour fluorescence intensity of the 6-AN group was much lower than that of the control. It was concordant with tumour size data (Fig. 6F). The result of IHC showed that the phospho-62 and Ki67 protein expression in the 6-AN group was reduced, while G6PD did not change significantly (Fig. 6G). Likewise, we observed that the tissular GSH levels were increased in the 6-AN treatment group (Fig. 6H). *G6PD* gene expression did not change significantly in the 6-AN group compared with the control. Similarly, 6-AN treatment caused *ATG7* upregulation (Fig. 6I), and the

autophagy-related protein BECN1 increased (Fig. 6J). These results showed that knockdown or inhibition of G6PD can cause autophagic death of tumour tissues, thereby inhibiting the occurrence and development of breast cancer.

Discussion

Despite the insightful understanding of metabolism and its influences on cancer during the past two decades, recent research has brought renewed awareness of cancer as a glucose metabolic disorder. The PPP is a major pathway for glucose catabolism, and it plays key roles in cell survival and proliferation [26]. Therefore, the activation of this pathway can supply tumour cells with nutrients to promote their survival and provide NADPH, an important source of detoxification of intracellular ROS, reductive biosynthesis and ribose biogenesis [27]. Because G6PD is the rate-limiting enzyme in the PPP and acts as a “gatekeeper” of this pathway, it was reported to promote local tumour growth and migration [28]. G6PD is overexpressed in various cancers, such as breast cancer, colorectal cancer, hepatoma, and lung cancer [10,29–31]. It was demonstrated that G6PD overexpression was associated with poor prognosis and drug resistance. For instance, NSD2 overexpression increases PPP flux by upregulating G6PD and HK2, thereby inducing tamoxifen-resistant breast cancer [32]. Moreover, a clinical study revealed that patients with G6PD overexpression had high recurrence risk and poor progression-free survival [29].

High G6PD expression promotes tumorigenesis and development, but its role in the metabolic microenvironment of breast cancer, especially in different molecular subtypes, is not yet clear. Two commonly studied human breast cancer cell lines were used, namely, MCF-7 and MDA-231, to explore whether G6PD could be a novel therapeutic target in the treatment of

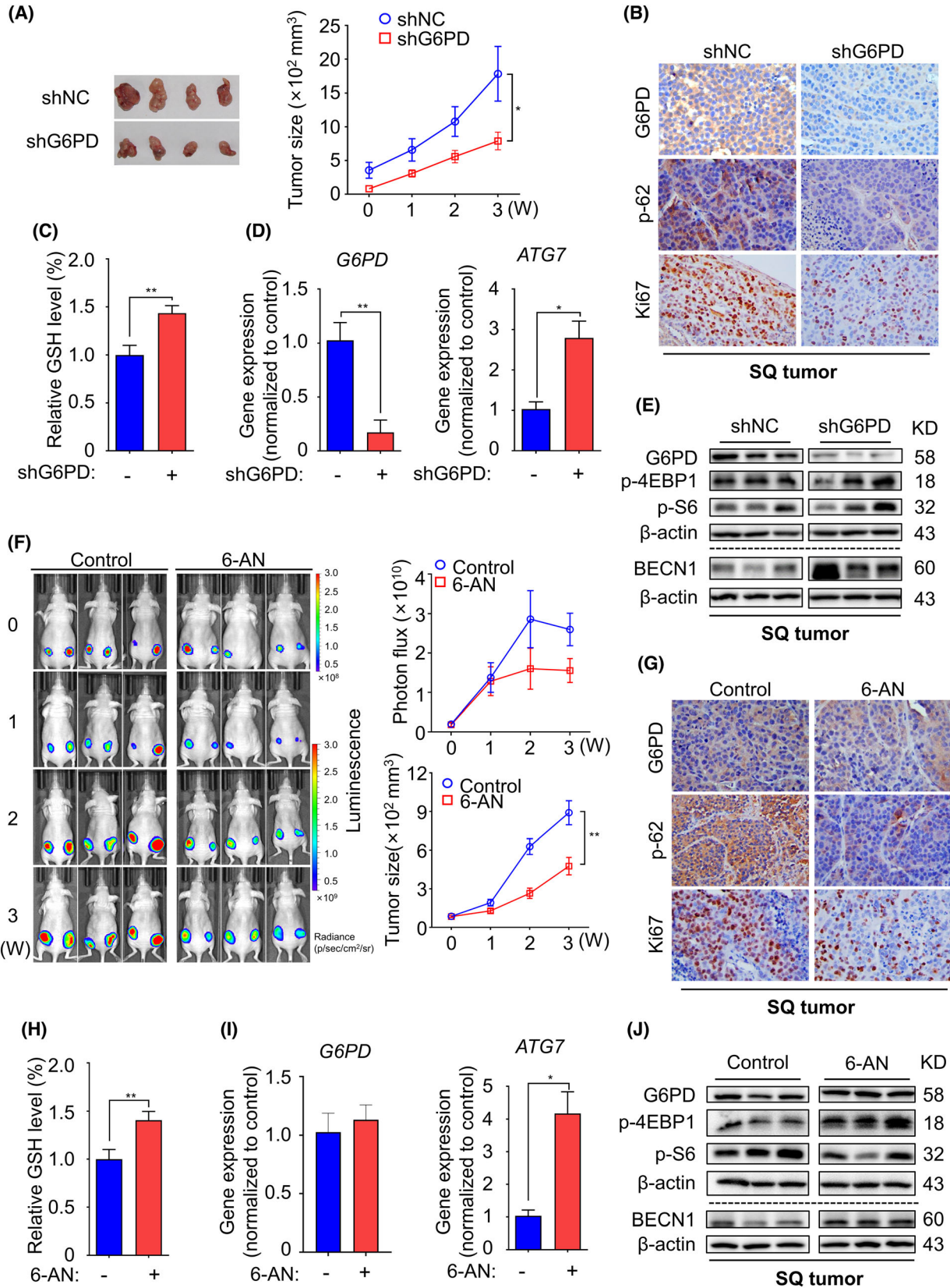


Fig. 6. Inhibition of G6PD suppresses tumour growth in preclinical models of breast cancer. (A) Orthotopic xenograft tumour size was measured in female CD1 nude mice with Vernier callipers ($n = 5$ in each group). (B) Paraffin-embedded tumour sections derived from MDA-231 cell-bearing mice were stained for G6PD, phospho-62, and Ki67. 400 \times magnification. (C) Relative GSH levels were measured in xenograft tumour tissues with G6PD knockdown. (D) The gene expression of *G6PD* and *ATG7* in xenograft tumour tissues was detected by q-PCR. (E) Immunoblot analysis of G6PD, BECN1, phospho-4EBP1, and phospho-S6 in xenograft tumours from mice injected with G6PD-knockdown cells. (F) Tumour-bearing mice were intraperitoneally administered either vehicle or 6-AN (5 mg·kg⁻¹, twice a week). Luminescence colour scale: 0 weeks (min = 3×10^7 , max = 3×10^9) and 1, 2, and 3 weeks (min = 3×10^8 , max = 3×10^9). The statistical graphs in the right panel indicate the photon flux of the tumour. Subcutaneous tumour size statistics after 20 days of mouse administration ($n = 5$ in each group). (G) IHC staining tests G6PD, phospho-62, and Ki67 in orthotopic tumours derived from MDA-231 cells treated with 6-AN. 400 \times magnification. (H) Relative GSH levels were measured in xenograft tumour tissues treated with 6-AN. (I) The gene expression of *G6PD* and *ATG7* in xenograft tumour tissues was detected by q-PCR. (J) Immunoblot analysis of G6PD, BECN1, phospho-4EBP1, and phospho-S6 in xenograft tumours from mice treated with 6-AN. * $P < 0.05$, ** $P < 0.01$.

breast cancer. In this study, our data suggest that G6PD downregulation can inhibit cell viability, escalate cell death, and decrease proliferation. Moreover, it has been demonstrated that restrained G6PD can compromise *in vitro* migration and colony formation, irrespective of whether G6PD is downregulated genetically or pharmaceutically. These results validated the importance of the PPP in the synthesis of biological macromolecules. Tumour cells were not able to obtain sufficient materials for nucleic acid synthesis via the PPP when the G6PD level decreased. Glucose is the major substrate for glucose metabolism, and elevated glucose uptake in MCF-7 and MDA-231 cells is primarily attributed to the glucose transporters GLUT3 and GLUT1. Our pre-experimental data indicate that inhibiting G6PD with 6-AN reduced GLUT3 expression in MCF-7 cells and GLUT1 expression in MDA-231 cells (data not shown).

ROS enhancement has been detected in several human cancers, and ROS show both pro-oncogenic and anti-oncogenic effects. For instance, ROS promote antitumor signalling and damage the redox balance of cells, thereby inducing cell death [33]. Conversely, ROS cause excessive cancerogenic signalling activation and incur genetic instability, which eventually leads to increased cell proliferation and enhanced viability [34]. Due to the paradoxical effect of redox balance between tumours and normal cells, tumour cells often express high levels of antioxidant factors that lead to ROS reduction, thus inhibiting cell death by establishing a new redox equilibrium [35]. After the degradation of the NSD2 protein, PPP flux suffocates and then inhibits tumour growth and survival by decreasing the production of NADPH and GSH and invoking elevated ROS to cause apoptosis [36]. It appears that the increased ROS levels have different effects on breast cancer subtypes. ROS can induce MCF-7 cell apoptosis and inhibit tumour cell viability. However, ROS promote cell migration and maintain cell viability in MDA-231 cells through the NF- κ B and TGF- β

signalling pathways [37]. We suspect that NADPH content could be reduced by inhibiting G6PD activity, which subsequently leads to overaccumulation of intracellular ROS and initiates cellular oxidative stress disturbances, followed by cell apoptosis. Flow cytometry data showed that 6-AN treatment caused a transient upregulation of ROS, and there was no significant change observed in cell apoptosis.

We further demonstrated that G6PD suppression in breast cancer cells may result in enhancement of the autophagy process and increase cell death and inhibition of cell proliferation and migration. Autophagy acts as an ROS and can induce cell death, but it can promote cell survival under metabolic stress [38]. In our research, 6-AN strongly activated autophagy, causing autophagic cell death.

In addition, our pre-experimental data showed that either inhibition of G6PD or genetic knockdown of G6PD reduced the gene and protein expression of ER α (data not shown). The oestrogen receptor ER α is a critical mediator of oestrogen action in cells. Previous studies pointed out that estradiol promoted the PPP in TSC2-deficient cells, resulting in increased glucose uptake in an AKT-dependent manner [39]. Moreover, oestrogen markedly promoted the proliferation of breast cancer cells in a dose-dependent manner [40]. These results suggest a strong correlation between oestrogen and G6PD.

In summary, targeting the PPP in MDA-231 and MCF-7 cells can weaken cell viability, inhibit proliferation, and decrease migration and colony formation by inducing cell autophagic death. Additionally, we speculate that oestrogen and glucose concentrations are also important factors involved in the G6PD-mediated PPP. These results provide a theoretical basis for a novel therapeutic strategy to incorporate G6PD-targeting therapy for systemic breast cancer treatment. Further large-scale clinical trials are warranted to evaluate the prognostic and predictive value of G6PD in breast cancer. Our research provides a theoretical basis

for understanding the mechanism of G6PD carcinogenesis and facilitates the search for new molecular mechanisms in breast cancer therapy.

Conclusions

In this study, we reported that targeting G6PD regulated PPP in MDA-231 and MCF-7 cells inhibit cell viability, survival, migration, and clone forming ability. G6PD inhibition induced up-regulation of ROS associated with autophagic cell death. *In vivo*, 6-AN treatment significantly impeded tumour growth in a xenograft model of breast cancer.

Collectively, our data suggest that G6PD plays a crucial role in tumorigenesis of breast cancer. This study provides new insights into the molecular mechanism of targeting G6PD in suppressing breast cancer, thus leading to the discovery of new therapy strategies.

Materials and methods

Cell lines and culture

The human breast cancer cell lines MDA-MB-231, MCF-7, MCF-10A, SKBR3, and 293T were purchased from (ATCC, Rockville, MD, USA). Cells were cultured in RPMI 1640 medium (MCF-7 and SKBR3) or DMEM medium (MDA-MB-231 and 293T) with 10% FBS and 1% penicillin/streptomycin. MCF-10A cells were grown in DMEM F-12 medium supplemented with 5% horse serum, 10 $\mu\text{g}\cdot\text{mL}^{-1}$ human insulin, 20 $\text{ng}\cdot\text{mL}^{-1}$ EGF, 100 $\text{ng}\cdot\text{mL}^{-1}$ cholera toxin, 0.5 $\mu\text{g}\cdot\text{mL}^{-1}$ hydrocortisone, and 1% penicillin/streptomycin. MCF-7 shNC/shG6PD and MDA-MB-231 shNC/shG6PD cells were established in our lab and cultured in the corresponding medium with 10% FBS, 1% penicillin/streptomycin, and 1% puromycin. All cultures were incubated at 37 °C in a humidified 5% CO₂ atmosphere.

Antibodies and reagents

The following chemicals were used: 6-AN, rapamycin (Cayman, Ann Arbor, MI, USA), chloroquine, H₂O₂, and NAC (Sigma, Burlington, MA, USA). Antibodies included G6PD, phospho-S6 (S235/236), cl-PARP, cl-caspase3, LC3B, phospho-62, phospho-4EBP1 (Cell Signalling Technologies, Danvers, MA, USA), BECN1, Nrf2 and β -actin (Santa Cruz, Dallas, TX, USA).

G6PD activity assay

G6PD activity was measured in cells using a Beyotime kit (G6PDH Activity Assay Kit with WST-8) (Shanghai, China) according to the manufacturer's instructions. Values were normalized to the protein content in each sample.

ROS levels

ROS levels were measured in cells using a Beyotime kit (Reactive Oxygen Species Assay Kit). Briefly, cells were incubated at 37 °C for 30 min in serum-free medium containing 10 μM DCFH-DA. Then, the cells were washed twice with PBS, treated with trypsin, and resuspended in PBS. Fluorescence was immediately measured using a FACScan Flow Cytometer.

Quantification of GSH

GSH was measured in cells using a Beyotime kit (GSH and GSSG Assay Kit) according to the manufacturer's instructions. Values were normalized to the cell quantity in each sample.

Colony formation assay

A total of 800–1000 cells per well were plated in 6-well plates and cultured for 24 h. The cells were treated with 6-AN for 24 h, and then the medium was replaced with 2% FBS fresh medium without 6-AN and incubated for 14 days. The cells were fixed in 10% formalin for 10 min and then stained with 0.05% crystal violet for 10 min. The number of colonies (containing ≥ 50 cells) was counted under a microscope.

Cell migration assay

A total of $8\text{--}10 \times 10^4$ cells per well were seeded in the upper chamber in 200 μL of serum-free medium or serum-free medium containing 6-AN, and 750 μL of 20% FBS medium was added to the lower chamber. After incubation at 37 °C for another 48 h, the cells were fixed in 10% formalin for 10 min and then stained with 0.05% crystal violet for 10 min.

Immunohistochemistry (IHC)

Paraffin-embedded tissue sections were dewaxed with xylene, rehydrated with an ethanol gradient, and then incubated with fresh 3% H₂O₂ (diluted with methanol) for 10 min to eliminate endogenous peroxidase activity. The slides were blocked with 10% goat serum (diluted with PBS) at room temperature for 30 min and incubated with primary antibodies at 4 °C overnight, followed by incubation with secondary antibodies at room temperature for 30 min. Subsequently, the sections were stained with 3,3-diaminobenzidine (DAB) for 5–10 min and counterstained with haematoxylin.

Cell transfection

The G6PD-overexpressing vector (pcG6PD) and its negative control vector (pcNC) were obtained from GenePharma (Shanghai, China) and transfected into cells using

Lipofectamine 2000 (Thermo Fisher Scientific, Waltham, MA, USA) according to the manufacturer's recommendation.

Stable cell line establishment

Short hair RNA (shRNA) used to silence G6PD (shG6PD) or control vector was transfected into 293T cells together with auxiliary plasmids (pLP1, pLP2 and VSV-G) to package the lentivirus. After infection with the lentivirus, breast cancer cells were screened out by adding puromycin to the media at a certain concentration. The shRNAs were designed and synthesized by GenePharma. The shG6PD cells were cultured with fresh medium containing $1 \mu\text{g}\cdot\text{mL}^{-1}$ puromycin daily.

Confocal microscopy

In this experiment, we used a GFP-RFP-LC3 tandem fluorescent plasmid to monitor the autophagy flux determined by changes in red fluorescence and green fluorescence at the same time and indicated by the GFP/RFP ratio. Cells were plated on coverslips and transiently transfected with the GFP-RFP-LC3 fusion plasmid for 6 h in serum-free medium by using Lipofectamine 2000. After incubating with 2% FBS culture medium for 12 h, the cells were treated with 6-AN or other drugs for 24 h. The cells were fixed with 10% formalin for 10 min and then stained with 4',6-diamino-2-phenylindole (DAPI) for 3 min, and the coverslips were sealed using 30% glycerin. Slides were sealed with nail polish and stored at 4°C in the dark. Finally, images were captured using a confocal microscope (Leica, Wilmington, DE, USA). Images were taken with a $63\times$ objective lens ($630\times$ magnification). The relative intensity of fluorescence was determined using IMAGEJ software (National Institutes of Health, Bethesda, MD, USA).

MTT assay

The MTT assay was carried out to determine cell viability. Briefly, $20 \mu\text{L}$ of MTT solution ($5 \text{ mg}\cdot\text{mL}^{-1}$) was added to each well. After incubation for 1–4 h, $100 \mu\text{L}$ of DMSO was added to each well and cultured at 37°C for 10 min. The absorbance was measured at $\text{OD} = 490 \text{ nm}$.

Cell death assay

A propidium iodide (PI) assay was carried out to determine cell death. Briefly, $100 \mu\text{L}$ of PI solution ($3 \mu\text{g}\cdot\text{mL}^{-1}$) was added to each well. After incubation for 45 min–1 h, the supernatant was aspirated. The absorbance was measured at $\text{OD} = 530$ and 620 nm .

q-PCR

Total RNA was isolated from cells by the RNAPrep Pure Cell/Bacteria Kit (TIANGEN, Beijing, China), and $2 \mu\text{g}$ of RNA

from each sample was reverse-transcribed to cDNA by the First-Strand cDNA Synthesis Kit (Thermo Fisher Scientific). cDNA ($0.5 \mu\text{g}$) of each sample was used as a template to perform PCR. The primer pairs for human genes were as follows:

G6PD, F: CGAGGCCGTCACCAAGAAC, R: GTAGTGGTCGATGCGGTAGA. *HMOX1*, F: AAGACTGCGTTCCTGCTCAAC, R: AAAGCCCTACAGCAACTGT CG. *NFE2L2*, F: TCCAGTCAGAAACCAGTGGAT, R: GAATGTCTGCGCCAAAAGCTG. *BECN1*, F: GGTG TCTCTCGCAGATTCATC, R: TCAGTCTTCGGCTGAGGTTCT. *ATG5*, F: AGAAGCTGTTTCGTCCTGT GG, R: AGGTGTTTCCAACATTGGCTC. *ATG7*, F: CTGCCAGCTCGCTTAACATTG, R: CTTGTTGAGG AGTACAGGGTTTT. *ATG12*, F: CTGCTGGCGACAC CAAGAAA, R: CGTGTCGCTCTACTGCC. *SQSTM1/P62*, F: GACTACGACTTGTGTAGCGTC, R: AGTGT CCGTGTTCACCTCC. *β -actin*, F: CACCATTGGCA ATGAGCGGTTTC, R: AGGTCTTTGCGGATGTC-CACGT.

Animal studies

Cells (5×10^6 cells in $100 \mu\text{L}$ of PBS) were injected subcutaneously into the bilateral mammary glands of nude mice. Primary tumours were assessed using bioluminescence imaging (BLI) every week. Tumour volumes were calculated by the formula $V (\text{mm}^3) = (\text{Length} \times \text{width}^2)/2$. The primary tumour tissue was removed. Tissues were fixed in 4% formaldehyde and prepared for histopathological evaluation.

For the intravenous model, 0.5 million cells in a volume of $100 \mu\text{L}$ were injected intravenously into the angular vein of BALB/c mice. Mice were given the substrate D-luciferin (PerkinElmer, Waltham, MA, USA) ($150 \text{ mg}\cdot\text{kg}^{-1}$) by intraperitoneal injection, and then an IVIS Spectrum instrument was used to monitor the lung colonization of tumour cells. Images were analysed by LIVING IMAGE SOFTWARE 4.5 (PerkinElmer, Waltham, MA, USA) through the photon flux of the BLI signal within a region.

Ethics approval and consent to participate

Animal experiments were performed according to the Guidelines on Laboratory Animals of Nankai University and were approved by the Institute Research Ethics Committee at Nankai University.

Statistical analysis

All data represent at least three experiments and shown as the mean \pm SEM. Measurements at single time points were analysed by ANOVA, and if they showed significance, they were further analysed by a two-tailed *t* test. All statistical tests were conducted using GRAPHPAD PRISM (GraphPad, San

Diego, CA, USA). The relative change in target proteins compared with β -actin levels was determined using IMAGEJ software. $P < 0.05$ was used to define statistical significance.

Acknowledgements

We would like to thank Gang Zhao (Department of Pathology, Tianjin Cancer Hospital) for supplying breast cancer sections, Miaomiao Sheng (Kunming University of Science and Technology) for providing breast cancer cell lines, and Xinying Wu (Animal Center of Nankai University) for technical support of *in vivo* imaging. This study was partially funded by “State Key Laboratory of Medicinal Chemical Biology (Nankai University, No. 2019014)” to C.W., “National Natural Science Foundation of China (81802080)” to D.L., “The Fundamental Research Funds for the Central Universities (Nankai University, #ZB19100128)” to C.L.

Conflict of interest

The authors declare no conflict of interest.

Author contributions

YL, FZ, YZ and DL designed, performed, and analysed the *in vivo* experiments. YL, FZ, FL, XH, QL, LY, TL, and YZ performed and analysed G6PD knockdown experiments *in vitro* and *in vivo*. YF, XP, XH, ZL, and JY provided guidance on data processing and writing. CL, YL, and CW contributed to the study design, implementation and supervision of the study. ZF, CW, QS, and CL contributed to the study design, supervised the study, and reviewed the manuscript. YL and CL wrote the manuscript. All authors had full access to the data and approved the final version of the manuscript.

Peer review

The peer review history for this article is available at <https://publons.com/publon/10.1111/febs.16614>.

Data availability statement

The authors confirm that the data supporting the findings of this study are available within the article. The raw data are available from the corresponding author on reasonable request.

References

- 1 Siegel RL, Miller KD, Jemal A. Cancer statistics, 2020. *CA Cancer J Clin.* 2020;**70**:7–30.
- 2 Esposito K, Chiodini P, Colao A. Metabolic syndrome and risk of cancer, meta analysis. *Diabetes Care.* 2012;**35**:2403–11.
- 3 Dibaba DT, Ogunsina K, Braithwaite D, Akinyemiju T. Metabolic syndrome and risk of breast cancer mortality by menopause, obesity, and subtype. *Breast Cancer Res Treat.* 2018;**174**:209–18.
- 4 Chen X, Xu Z, Zhu Z, Chen A, Fu G, Wang Y, et al. Modulation of G6PD affects bladder cancer via ROS accumulation and the AKT pathway *in vitro*. *Int J Oncol.* 2018;**53**:1703–12.
- 5 Du W, Jiang P, Mancuso A, Stonestrom A, Brewer MD, Minn AJ, et al. TAp73 enhances the pentose phosphate pathway and supports cell proliferation. *Nat Cell Biol.* 2013;**15**:991–1000.
- 6 Wu S, Wang H, Li Y, Xie Y, Huang C, Zhao H, et al. Transcription factor YY1 promotes cell proliferation by directly activating the pentose phosphate pathway. *Cancer Res.* 2018;**78**:4549–62.
- 7 Cui J, Pan Y, Wang J, Liu Y, Wang H, Li H. MicroRNA-206 suppresses proliferation and predicts poor prognosis of HR-HPV-positive cervical cancer cells by targeting G6PD. *Oncol Lett.* 2018;**16**:5946–52.
- 8 Zhang Q, Yi X, Yang Z, Han Q, Di X, Chen F, et al. Overexpression of G6PD represents a potential prognostic factor in clear cell renal cell carcinoma. *J Cancer.* 2017;**8**:665–73.
- 9 Yang HC, Wu YH, Yen WC, Liu HY, Hwang TL, Stern A, et al. The redox role of G6PD in cell growth, cell death, and cancer. *Cells.* 2019;**8**:1055.
- 10 Ju HQ, Lu YX, Wu QN, Liu J, Zeng ZL, Mo HY, et al. Disrupting G6PD-mediated redox homeostasis enhances chemosensitivity in colorectal cancer. *Oncogene.* 2017;**36**:6282–92.
- 11 Zhang HS, Zhang ZG, Du GY, Sun HL, Liu HY, Zhou Z, et al. Nrf2 promotes breast cancer cell migration via up-regulation of G6PD/HIF-1 α /Notch1 axis. *J Cell Mol Med.* 2019;**23**:3451–63.
- 12 Hamilton NM, Dawson M, Fairweather EE, Hamilton NS, Hitchin JR, James DI, et al. Novel steroid inhibitors of glucose 6-phosphate dehydrogenase. *J Med Chem.* 2012;**55**:4431–45.
- 13 Mele L, Paino F, Papaccio F, Regad T, Boocock D, Stiuso P, et al. A new inhibitor of glucose-6-phosphate dehydrogenase blocks pentose phosphate pathway and suppresses malignant proliferation and metastasis *in vivo*. *Cell Death Dis.* 2018;**9**:572.
- 14 Wang X, Wu G, Cao G, Yang L, Xu H, Huang J, et al. Zoledronic acid inhibits the pentose phosphate pathway through attenuating the Ras-TAp73-G6PD axis in bladder cancer cells. *Mol Med Rep.* 2015;**12**:4620–5.
- 15 Köhler EBH, Neubert D. Inhibition of NADP dependent oxidoreductases by the 6-aminonicotinamide analogue of NADP. *FEBS Lett.* 1970;**6**:225–8.

- 16 Barajas JM, Reyes R, Guerrero MJ, Jacob ST, Motiwala T, Ghoshal K. The role of miR-122 in the dysregulation of glucose-6-phosphate dehydrogenase (G6PD) expression in hepatocellular cancer. *Sci Rep.* 2018;**8**:9105.
- 17 He C, Yang J, Ding J, Li S, Wu H, Xiong Y, et al. Downregulation of glucose-6-phosphate dehydrogenase by microRNA1 inhibits the growth of pituitary tumor cells. *Oncol Rep.* 2018;**40**:3533–42.
- 18 Zhang Z, Liew CW, Handy DE, Zhang Y, Leopold JA, Hu J, et al. High glucose inhibits glucose-6-phosphate dehydrogenase, leading to increased oxidative stress and beta-cell apoptosis. *FASEB J.* 2010;**24**:1497–505.
- 19 Mele L, la Noce M, Paino F, Regad T, Wagner S, Liccardo D, et al. Glucose-6-phosphate dehydrogenase blockade potentiates tyrosine kinase inhibitor effect on breast cancer cells through autophagy perturbation. *J Exp Clin Cancer Res.* 2019;**38**:160.
- 20 Leopold JA, Cap A, Scribner AW, Stanton RC, Loscalzo J. Glucose-6-phosphate dehydrogenase deficiency promotes endothelial oxidant stress and decreases endothelial nitric oxide bioavailability. *FASEB J.* 2001;**15**:1771–3.
- 21 Luo Z, Xu X, Sho T, Zhang J, Xu W, Yao J, et al. ROS-induced autophagy regulates porcine trophectoderm cell apoptosis, proliferation, and differentiation. *Am J Physiol Cell Physiol.* 2019;**316**:C198–209.
- 22 Lee JW, Choi AH, Ham M, Kim JW, Choe SS, Park J, et al. G6PD up-regulation promotes pancreatic beta-cell dysfunction. *Endocrinology.* 2011;**152**:793–803.
- 23 Nadeem A, Al-Harbi NO, Ahmad SF, Ibrahim KE, Siddiqui N, Al-Harbi MM. Glucose-6-phosphate dehydrogenase inhibition attenuates acute lung injury through reduction in NADPH oxidase-derived reactive oxygen species. *Clin Exp Immunol.* 2018;**191**:279–87.
- 24 Parsanathan R, Jain SK. Glucose-6-phosphate dehydrogenase deficiency increases cell adhesion molecules and activates human monocyte-endothelial cell adhesion: protective role of l-cysteine. *Arch Biochem Biophys.* 2019;**663**:11–21.
- 25 Ham MCS, Shin KC, Choi G, Kim JW, Noh JR, Kim YH, et al. Glucose-6-phosphate dehydrogenase deficiency improves insulin resistance with reduced adipose tissue inflammation in obesity. *Diabetes.* 2016;**65**:2624–38.
- 26 Shin E, Koo JS. Glucose metabolism and glucose transporters in breast cancer. *Front Cell Dev Biol.* 2021;**9**:728759.
- 27 Jiang P, Du W, Wu M. Regulation of the pentose phosphate pathway in cancer. *Protein Cell.* 2014;**5**:592–602.
- 28 Jiang P, Du W, Wang X, Mancuso A, Gao X, Wu M, et al. p53 regulates biosynthesis through direct inactivation of glucose-6-phosphate dehydrogenase. *Nat Cell Biol.* 2011;**13**:310–6.
- 29 Pu H, Zhang Q, Zhao C, Shi L, Wang Y, Wang J, et al. Overexpression of G6PD is associated with high risks of recurrent metastasis and poor progression-free survival in primary breast carcinoma. *World J Surg Oncol.* 2015;**13**:323–7.
- 30 Zhang X, Gao F, Ai H, Wang S, Song Z, Zheng L, et al. TSP50 promotes hepatocyte proliferation and tumour formation by activating glucose-6-phosphate dehydrogenase (G6PD). *Cell Prolif.* 2021;**54**:e13015.
- 31 Nagashio R, Oikawa S, Yanagita K, Hagiuda D, Kuchitsu Y, Igawa S, et al. Prognostic significance of G6PD expression and localization in lung adenocarcinoma. *Biochim Biophys Acta Proteins Proteom.* 2019;**1867**:38–46.
- 32 Wang J, Duan Z, Nugent Z, Zou JX, Borowsky AD, Zhang Y, et al. Reprogramming metabolism by histone methyltransferase NSD2 drives endocrine resistance via coordinated activation of pentose phosphate pathway enzymes. *Cancer Lett.* 2016;**378**:69–79.
- 33 Villalpando-Rodriguez GE, Gibson SB. Reactive oxygen species (ROS) regulates different types of cell death by acting as a rheostat. *Oxid Med Cell Longev.* 2021;**2021**:9912436.
- 34 Mittler R. ROS are good. *Trends Plant Sci.* 2017;**22**:11–9.
- 35 Martinez-Reyes I, Cuezva JM. The H(+)-ATP synthase: a gate to ROS-mediated cell death or cell survival. *Biochim Biophys Acta.* 2014;**1837**:1099–112.
- 36 Wang Q, Zheng J, Zou JX, Xu J, Han F, Xiang S, et al. S-adenosylhomocysteine (AdoHcy)-dependent methyltransferase inhibitor DZNep overcomes breast cancer tamoxifen resistance via induction of NSD2 degradation and suppression of NSD2-driven redox homeostasis. *Chem Biol Interact.* 2020;**317**:108965.
- 37 Chen C, Wang S, Liu P. Deferoxamine enhanced mitochondrial iron accumulation and promoted cell migration in triple-negative MDA-MB-231 breast cancer cells via a ROS-dependent mechanism. *Int J Mol Sci.* 2019;**20**:4952.
- 38 Onorati AV, Dyczynski M, Ojha R, Amaravadi RK. Targeting autophagy in cancer. *Cancer.* 2018;**124**:3307–18.
- 39 Sun Y, Gu X, Zhang E, Park MA, Pereira AM, Wang S, et al. Estradiol promotes pentose phosphate pathway addiction and cell survival via reactivation of Akt in mTORC1 hyperactive cells. *Cell Death Dis.* 2014;**5**:e1231.
- 40 Li Y, Jiang B, Wu X, Huang Q, Chen W, Zhu H, et al. Long non-coding RNA MIAT is estrogen-responsive and promotes estrogen-induced proliferation in ER-positive breast cancer cells. *Biochem Biophys Res Commun.* 2018;**503**:45–50.